

Molecular dynamics insights into limited impact of nanoscale defects on lithocholic acid adsorption on graphene

Rui-Jian Yang(杨瑞建) and Zhi-Gang Shao(邵志刚)
Citation: Chin. Phys. B, 2026, 35 (**7**): 076803. DOI: 10.1088/1674-1056/ae504e
http://cpb.iphy.ac.cn; http://iopscience.iop.org/cpb

What follows is a list of articles you may be interested in

Formation of crystalline Si_9C_{15} nano-islands and Si_9C_{15}/graphene heterostructures on Ru(0001)

Lijing Huang(黄丽静), Yumeng Li(李雨萌), Hongqin Xiao(肖洪钦), Yuxuan He(何昱萱), Geng Li(李更), and Hong-Jun Gao(高鸿钧)
Chin. Phys. B, 2026, 35 (**5**): 056801. DOI: 10.1088/1674-1056/ae4c6f

Second-order topological insulator in twisted bilayer graphene with small twist angles

Fenghua Qi(戚凤华), Jie Cao(曹杰), Xingfei Zhou(周兴飞), and Guojun Jin(金国钧)
Chin. Phys. B, 2025, 34 (**11**): 116801. DOI: 10.1088/1674-1056/adee03

Bond-resolved silicene on Au(111) substrate

Ye Chen(陈烨), Wenya Zhai(翟文雅), Haoyuan Zang(臧浩原), Zengfu Ou(欧增福), Donghui Guo(郭东辉), and Jingcheng Li(李竟成)
Chin. Phys. B, 2025, 34 (**9**): 096801. DOI: 10.1088/1674-1056/adee02

Combining machine learning algorithms with traditional methods for resolving the atomic-scale dynamic structure of monolayer MoS_2 in high-resolution transmission electron microscopy

Yu Meng(蒙宇), Shuya Wang(王淑雅), Xibiao Ren(任锡标), Han Xue(薛涵), Xuejun Yue(岳学军), Chuanhong Jin(金传洪), Shanggang Lin(林上港), and Fang Lin(林芳)
Chin. Phys. B, 2025, 34 (**1**): 016802. DOI: 10.1088/1674-1056/ad9ba3

Controlled fabrication of freestanding monolayer SiC by electron irradiation

Yunli Da(笪蕴力), Ruichun Luo(罗瑞春), Bao Lei(雷宝), Wei Ji(季威), and Wu Zhou(周武)
Chin. Phys. B, 2024, 33 (**8**): 086802. DOI: 10.1088/1674-1056/ad6132

Molecular dynamics insights into limited impact of nanoscale defects on lithocholic acid adsorption on graphene

Rui-Jian Yang(杨瑞建)[1] and Zhi-Gang Shao(邵志刚)[1,2,†]

[1] *Guangdong Basic Research Center of Excellence for Structure and Fundamental Interactions of Matter, Guangdong Provincial Key Laboratory of Quantum Engineering and Quantum Materials, School of Physics, South China Normal University, Guangzhou* 510006, *China*

[2] *Guangdong–Hong Kong Joint Laboratory of Quantum Matter, Frontier Research Institute for Physics, South China Normal University, Guangzhou* 510006, *China*

(Received 19 September 2025; revised manuscript received 2 February 2026; accepted manuscript online 11 March 2026)

Lithocholic acid (LCA), a bile acid metabolite with demonstrated lifespan-extension capabilities, holds considerable biomedical promise. The development of nano-enabled platforms, such as those based on two-dimensional (2D) materials, is crucial to empower its future applications in drug delivery and sensing. For fundamental mechanistic studies, graphene serves as an ideal model system owing to its structural simplicity and computational tractability, which allow for precise control and reliable simulation of its surface properties, such as through defect engineering. However, the adsorption behavior of LCA on graphene surfaces, particularly the mechanistic role of surface defects that are central to tailoring material properties, remains inadequately characterized. To elucidate the underlying physical principles governing this interaction, we employed molecular dynamics simulations to systematically compare LCA binding on ideal graphene (I-Gra) and a series of defective graphene (D-Gra) models with varying defect sizes and edge chemistries. Our results reveal that the binding free energy of LCA converges to a similar value across all surfaces, indicating a limited impact of nanoscale defects. Structural analysis shows that while hydrophilic defect edges form strong, localized hydrogen bonds with water, the overall architecture of the interfacial hydration layer remains largely preserved. This confinement of defect influence leads to minimal variation in the non-polar solvation free energy, the key thermodynamic term governing hydrophobic adsorption. Consequently, the adsorption strength exhibits remarkable robustness against the investigated defects. These findings elucidate a defect-insensitive adsorption mechanism, highlighting that the continuous hydrophobic graphene plane, not localized defect features, dominates the interaction. This insight provides a crucial theoretical foundation for predicting the performance of realistic, non-ideal graphene interfaces in LCA-related biomedical applications.

Keywords: lithocholic acid, graphene, molecular dynamics simulation, defect engineering, binding free energy

PACS: 68.65.Pq, 68.43.–h, 87.15.A–, 68.08.Bc

DOI: 10.1088/1674-1056/ae504e **CSTR:** 32038.14.CPB.ae504e

1. Introduction

Lithocholic acid, a key member of the bile acid family, plays critical physiological roles in biological systems, including cholesterol metabolism regulation and bile acid homeostasis.[1–6] Notably, breakthrough studies have recently revealed that LCA mimics caloric restriction effects, with experimental validation demonstrating its lifespan-extending capabilities in model organisms such as mice, nematodes, and fruit flies.[7,8] To realize the biomedical potential of LCA, efficient platforms for its delivery and sensing are essential. Two-dimensional (2D) materials have emerged as a unique class of nanomaterials for such applications, owing to their exceptional properties including ultra-high surface area, tunable surface chemistry, and outstanding mechanical strength.[9–13] Among these, graphene represents a paradigmatic 2D material. Its well-defined, atomically flat structure and extensive history in both experimental and computational studies of biomolecular interactions make it a highly suitable and widely adopted model system for investigating fundamental interfacial phenomena at solid–liquid interfaces.[14–21] Critically, defect engineering enables precise modulation of graphene's physicochemical characteristics, such as surface hydrophilicity/hydrophobicity and charge distribution, thereby creating new opportunities for expanded biomedical utility.[22–27] However, the extent to which such nanoscale modifications translate into measurable changes in the adsorption thermodynamics of small biomolecules remains a fundamental question, crucial for predicting the behavior of real, non-ideal graphene surfaces.

While graphene interactions with biomacromolecules (such as proteins and DNA) have been systematically investigated,[28–35] for instance, Li *et al*. employed molecular dynamics simulations to elucidate the role of defects in protein adsorption,[36] and Gao *et al*. explored mechanisms governing dsDNA interactions with ideal and defective graphene,[23] the dynamic adsorption behavior of small biomolecules at

†Corresponding author. E-mail: zgshao@scnu.edu.cn

© 2026 Chinese Physical Society and IOP Publishing Ltd. All rights, including for text and data mining, AI training, and similar technologies, are reserved.

graphene interfaces remains inadequately characterized. Understanding the adsorption behavior of LCA on pristine and defective graphene surfaces is essential to elucidate interfacial interaction mechanisms in biological systems and develop graphene-based drug delivery systems and biosensors. Specifically, a detailed understanding of LCA–graphene binding at the molecular level is crucial. Equally important is to quantify how nanoscale defects, varying in size and edge chemistry, affect the adsorption strength and mechanism. This knowledge is pivotal for advancing reliable graphene-based platforms, especially for applications like drug delivery where material imperfections are intrinsic.

This study employs molecular dynamics simulations and free energy calculations to systematically investigate the adsorption of LCA on I-Gra and a series of D-Gra models with controlled pore sizes and edge chemistries, aiming to elucidate the extent to which such nanoscale defects modulate the adsorption thermodynamics and mechanism. Based on 400-ns simulations, we analyzed the binding kinetics, contact area, and interaction energy for the representative I-Gra and a specific defect model, D-Gra1.0. To comprehensively assess the thermodynamic impact of defects, we further computed the binding free energy and its components for a total of five systems, including I-Gra, D-Gra1.0, and three additional variants: D-Gra0.5, D-Gra1.5, and D-Gra1.0h. The results quantify the contribution of various energy terms and reveal how the interfacial hydration structure responds to defects. This work provides a systematic assessment of how different defect parameters, size and edge chemistry, govern the adsorption of LCA on graphene, offering crucial insights for predicting the performance of graphene-based materials with inherent nanoscale imperfections.

2. Model and method

The graphene systems comprising five distinct models, I-Gra and four D-Gra variants with systematically varied pore sizes and edge chemistries, were constructed as follows (Fig. 1). I-Gra, which measured 3.7 nm × 4.4 nm (662 carbon atoms), was modeled with uncharged Lennard–Jones particles, and the van der Waals parameters were set as $\sigma = 0.34$ nm, $\varepsilon_{cc} = 0.36$ kJ/mol.[37] The primary defective model, D-Gra1.0, was engineered by introducing a 1-nm diameter circular pore at the center of the I-Gra lattice, with the pore periphery comprising 12 carbon atoms. To passivate edge dangling bonds and impart specific chemical functionalities, these peripheral carbon atoms were terminated with charged carboxyl groups (–COO^-) and hydrogen atoms (–H) in alternating positions.[36] To comprehensively investigate the effect of defect geometry and chemistry, three additional variants were constructed based on the same modeling approach: D-Gra0.5, featuring a 0.5-nm diameter pore with its 6 peripheral atoms passivated by one –COO^- and five –H atoms; D-Gra1.5, featuring a 1.5-nm diameter pore with its 18 peripheral atoms alternately terminated with –COO^- and –H; and D-Gra1.0h, featuring a 1.0-nm diameter pore with all 12 peripheral atoms terminated solely by –H atoms, creating a purely hydrophobic defect edge. Following molecular modeling, LCA underwent structural optimization and subsequent RESP (restrained electrostatic potential) atomic charge computation to achieve force field parameterization.[38–40]

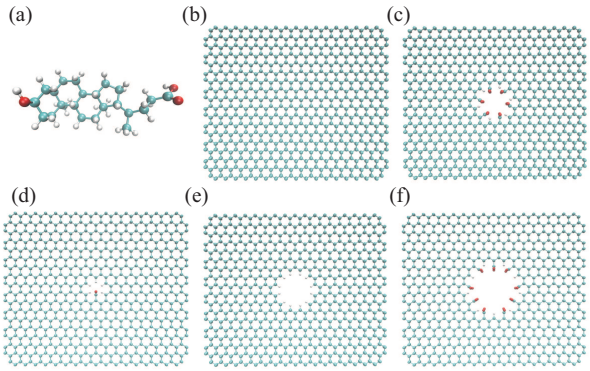


Fig. 1. Atomic configurations of all simulated systems. (a) LCA molecule, (b) I-Gra, (c)–(f) defective graphene models with systematically varied pore sizes and edge chemistry: (c) D-Gra1.0 (1.0 nm pore, –COO^-/–H edges), (d) D-Gra0.5 (0.5 nm pore, one –COO^-), (e) D-Gra1.0h (1.0 nm pore, fully hydrogenated edges), and (f) D-Gra1.5 (1.5 nm pore, –COO^-/–H edges).

All simulations were performed using the GROMACS package and the force field was described using AMBER99SB.[41,42] VMD software was utilized for visualizing the structure.[43] For each system, a simulation box of dimensions 6 nm × 5.5 nm × 6 nm was constructed. The graphene sheet was centered in the *xy*-plane, with the LCA molecule initially placed 1.5 nm above it. Systems were solvated with TIP3P water.[44] Periodic boundary conditions were used in the simulation process. To maintain electrical neutrality, sodium ions (Na^+) were added to neutralize the net negative charge carried by the deprotonated carboxyl groups on the graphene edges where applicable. Specifically, 6 Na^+ ions were added to the D-Gra1.0 system to neutralize its six –COO^- groups. Similarly, 1 Na^+ and 9 Na^+ ions were added to neutralize the single –COO^- in D-Gra0.5 and the nine –COO^- groups in D-Gra1.5, respectively. The electrically neutral I-Gra and D-Gra1.0h systems did not require additional ions for charge neutralization. Covalent bond lengths involving hydrogen atoms were constrained by the LINCS algorithm.[45] Remote electrostatic interactions were calculated by the particle mesh Ewald (PME) method, and van der Waals interactions used a 1.2-nm cutoff.[46,47] The time step was set to 2.0 fs, and data were collected every 100 ps. After energy minimization, each system was pre-equilibrated for 1000 ps using the Berendsen coupling method at a constant temperature of 300 K. Following energy minimization, all simulated systems underwent equilibration within the NVT ensemble,

maintaining temperature at 300 K via the v-rescale thermostat while regulating system pressure to 1 bar (1 bar = 10^5 Pa) using the Parrinello–Rahman barostat.[48,49] Subsequently, a production simulation was performed for 400 ns in the NVT ensemble. The binding free energies were calculated using the MM–PBSA approach as implemented in the gmx_MMPBSA tool.[50] The simulation protocols described above apply to the five primary systems in pure water. Additional control simulations, including those at physiological ionic strength (0.15-M NaCl) and with hydrogenated outer edges of the graphene sheet, were performed to test the robustness of the findings; their specific setups are detailed in the supporting information (Sections S4 and S5).

3. Results and discussion

3.1. The interaction between LCA molecules and I-Gra

Based on the analysis of configuration diagrams at key time points during the simulation (as shown in Fig. 2), we examined the dynamic adsorption process of LCA molecules on the I-Gra surface. Initially ($t = 0$ ns), the molecules were positioned 1.5 nm above the center of the I-Gra plane. Over the 400-ns simulation period, continuous migration of the molecules across the I-Gra surface was observed.

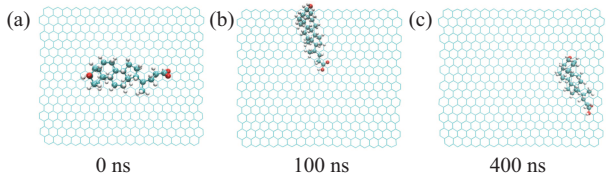


Fig. 2. Conformational diagrams of LCA molecules and I-Gra at different critical moments during the simulation process: (a) 0 ns, (b) 100 ns, (c) 400 ns.

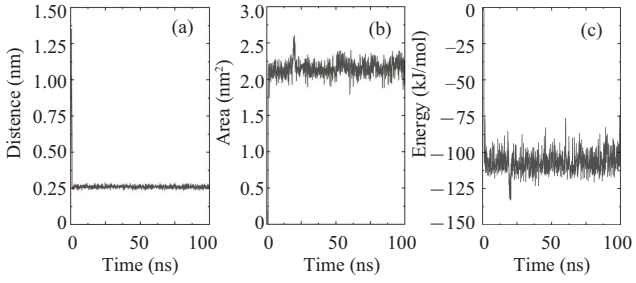


Fig. 3. (a) Time evolution of the vertical distance between LCA centroid and I-Gra plane, (b) time evolution of the contact area between LCA molecule and the I-Gra plane, and (c) time evolution of the van der Waals interaction energy between LCA molecule and the I-Gra plane.

The analysis of the vertical distance between the molecular centroid and the I-Gra plane (shown in Fig. 3) revealed a rapid decrease in the early simulation stage, followed by gradual stabilization. Concurrently, the contact area between the molecule and I-Gra increased sharply from 0 nm^2 to approximately 2.1 nm^2 within the initial simulation phase before reaching equilibrium. Correspondingly, the van der Waals interaction energy decreased rapidly from 0 kJ/mol to approximately −108 kJ/mol and subsequently stabilized. These kinetic data collectively demonstrate that LCA molecules undergo rapid initial adsorption on the I-Gra surface, followed by stabilization while retaining migration capability post-adsorption, characteristic of a dynamic adsorption process.

3.2. The interaction between LCA molecules and D-Gra1.0

Based on the same analytical methodology, we investigated the adsorption behavior of LCA on the D-Gra1.0 surface. The analysis of the system conformation at distinct simulation time points (see Fig. 4) revealed that at the initial stage ($t = 0$ ns), LCA molecules were positioned approximately 1.5 nm above the center of the D-Gra plane. Throughout the subsequent 400-ns simulation, the molecules exhibited continuous migration across the D-Gra surface. Analysis of the time evolution of the vertical distance between the LCA molecular centroid and the D-Gra plane (see Fig. 5) revealed that this distance exhibited brief initial fluctuations, followed by a rapid decrease, and subsequently approached a relatively stable state with persistent minor oscillations, similar to the behavior observed on I-Gra. The adsorption process was predominantly stable, with a transient event occurring around 91 ns.

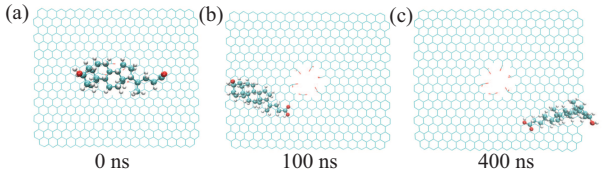


Fig. 4. Conformational diagrams of LCA molecule and D-Gra1.0 at different critical moments during the simulation process (a) 0 ns, (b) 100 ns, and (c) 400 ns.

At this time, a synchronous decrease in contact area (from 2.65 nm^2 to 2.25 nm^2) and a corresponding weakening of the van der Waals interaction energy (from −145 kJ/mol to −105 kJ/mol) were observed (Fig. 5).

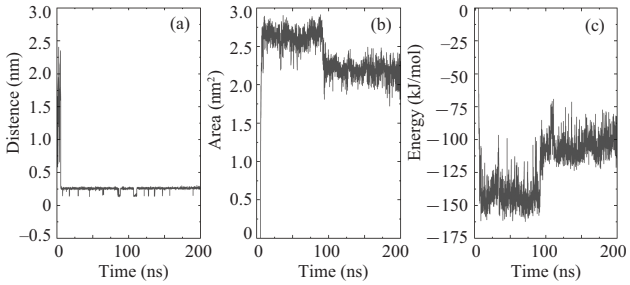


Fig. 5. (a) Time evolution of the vertical distance between LCA centroid and D-Gra plane, (b) time evolution of the contact area between LCA molecule and the D-Gra plane, (c) time evolution of the van der Waals interaction energy between LCA molecule and the D-Gra plane.

Structural snapshots and root-mean-square deviation (RMSD) analysis (see Figs. 6 and 7) indicate that this corresponds to a transient conformational folding rearrangement of the LCA molecule. This rearrangement led to a more compact LCA structure, temporarily reducing its contact interface with the graphene. Notably, after this short-lived event, the

molecule quickly re-established a stable adsorbed state, and both the vertical distance and interaction energy remained stable for the remainder of the simulation. The final contact area (2.25 nm^2) and interaction energy level are comparable to those on I-Gra, suggesting a similar overall strength of physical adsorption. This indicates that while local molecular rearrangements can occur, they do not compromise the long-term stability of adsorption on the graphene surface.

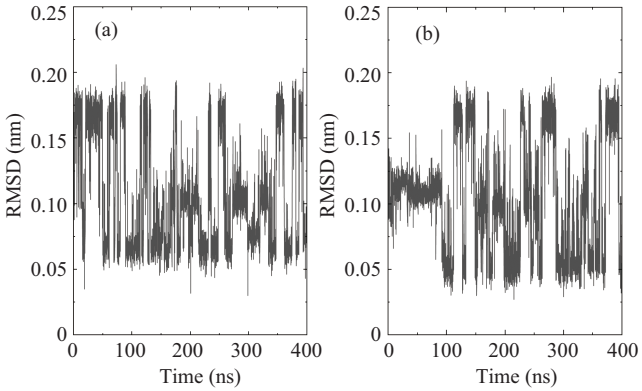


Fig. 6. (a) The relationship between the root-mean-square deviation of LCA in the I-Gra system and time, (b) The relationship between the root-mean-square deviation of LCA in the D-Gra1.0 system and time.

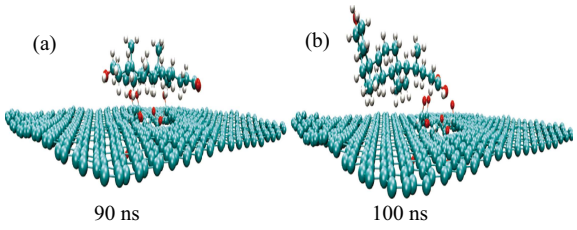


Fig. 7. (a) The structural diagram of the LCA molecule at the 90-ns time point, (b) the structural diagram of the LCA molecule at the 100-ns time point.

3.3. Convergence of binding free energy across diverse graphene defects

To quantitatively elucidate the thermodynamic driving forces for LCA adsorption and to probe the generalizability of defect effects, we calculated the binding free energy using the MM–PBSA method for five graphene systems: I-Gra, D-Gra1.0, D-Gra0.5, D-Gra1.5, and D-Gra1.0h. The calculations were performed using trajectories from the stable binding phase (100 ns–200 ns). The binding free energy is decomposed into molecular mechanics terms (van der Waals energy and electrostatic interaction energy) and solvation terms (polar solvation free energy, and non-polar solvation free energy). Key results for all systems are summarized in Fig. 8(a).

The analysis of the decomposed terms reveals consistent patterns. The van der Waals interaction provides the dominant favorable contribution across all systems. As expected, systems with carboxylated edges (D-Gra1.0, D-Gra0.5, D-Gra1.5) exhibit additional favorable electrostatic interactions, which are largely absent in I-Gra. A minimal electrostatic contribution (-0.07 kcal/mol) is also observed in D-Gra1.0h, likely arising from the subtle polarization of the C–H bonds at the defect edge. However, these electrostatic gains are consistently counterbalanced by more unfavorable polar solvation penalties.

The most critical finding is the near invariance of the non-polar solvation free energy, which fluctuates within a negligible range of -1.82 kcal/mol to -1.87 kcal/mol across all five systems (see Fig. 8(a)). This term, which encapsulates the thermodynamic cost of dehydrating the hydrophobic interface upon adsorption, is remarkably insensitive to the presence, size, or chemical termination of the nanoscale defects. Consequently, the total binding free energies for all systems converge to a highly similar value, ranging from -26.5 kcal/mol to -27.8 kcal/mol. This convergence indicates a saturation effect in adsorption strength, governed by a common thermodynamic bottleneck. The structural origin of this invariant non-polar solvation free energy is investigated in the following section.

3.4. Analysis of interfacial hydration structure reveals localized defect effects

To uncover the structural origin of the invariant non-polar solvation free energy observed in Subsection 3.3, we analyzed the organization of interfacial water by calculating the radial distribution function (RDF) between all atoms of the graphene sheet (including edge functional groups) and water oxygen atoms.

The radial distribution functions (RDFs) for I-Gra and the fully hydrogenated defect model D-Gra1.0h are nearly superimposable, particularly at distances beyond the first hydration shell ($r > 0.35$ nm), as shown in Fig. 8(b). This close overlap demonstrates that a nanoscale pore with a hydrophobic edge does not disrupt the overall architecture of the interfacial water layer adjacent to the extended graphene plane. The structural preservation is consistent with the nearly identical non-polar solvation free energy observed for these two systems. The detailed adsorption dynamics and conformational evolution of LCA on D-Gra1.0h, which further confirm its behavioral similarity to I-Gra, are provided in the supporting information (Section S2).

In contrast, defects with charged edges introduce a distinct structural feature: a sharp peak at approximately $r \approx 0.25$ nm (the inset of Fig. 8(b)). This peak is unambiguously attributed to water molecules forming strong, localized hydrogen bonds with the edge –COO^- groups. The intensity of this characteristic peak scales directly with the number of hydrophilic sites. It is most pronounced for D-Gra1.5 (nine –COO^- groups; Fig. S9(b)), clearly visible for D-Gra1.0 (six groups; Fig. 8(b)), and subtle for D-Gra0.5 (a single group; Fig. S3(b)). This systematic variation underscores the highly localized nature of the defect's influence. The complete kinetic profiles and structural analyses for the D-Gra0.5 and D-

Gra1.5 systems are documented in Sections S1 and S3 of the supporting information, respectively.

This contrast provides direct structural evidence that the influence of hydrophilic defects is confined to the immediate vicinity of the defect edges. While these edges create a significant local perturbation in water structure, this perturbation decays rapidly with distance and does not propagate to reorganize the broader interfacial water network responsible for the hydrophobic effect. Therefore, the thermodynamic cost of dehydrating this predominant interface, the non-polar solvation free energy, remains unchanged, leading to the convergence in total binding affinity. In summary, the adsorption is dominated by the continuous hydrophobic plane, with nanoscale defects exerting only a local, thermodynamically insignificant influence.

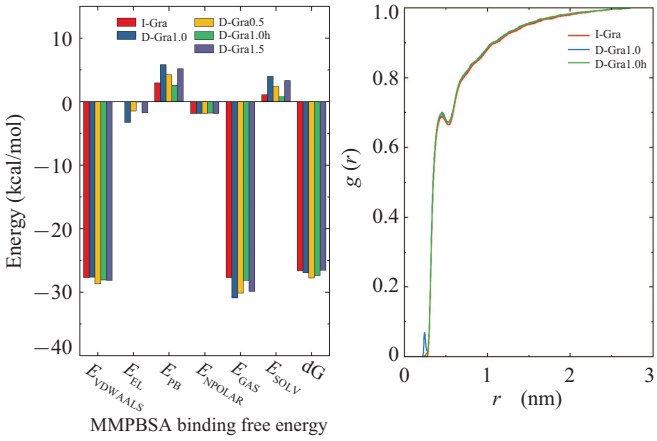


Fig. 8. (a) The binding free energy of LCA with the five graphene systems and its decomposed components, (b) radial distribution functions between atoms of the graphene sheet and water oxygen atoms for I-Gra, D-Gra1.0, and D-Gra1.0h.

4. Conclusions

Through systematic molecular dynamics simulations, we investigated the adsorption of LCA on ideal and defective graphene, varying defect size and edge chemistry. The binding free energy of LCA converges to a similar value across all surfaces, demonstrating remarkable insensitivity to nanoscale defects. This convergence is primarily dictated by the near-invariance of the non-polar solvation free energy, the key thermodynamic term governing hydrophobic interactions. Structural analysis of the interfacial water layer via radial distribution functions provides the foundation for this observation: while hydrophilic defect edges form strong, localized hydrogen bonds, the global architecture of the hydration layer adjacent to the extended graphene plane remains preserved. Consequently, the thermodynamic cost of dehydrating this interface, the non-polar solvation free energy, shows negligible variation, leading directly to the observed convergence in overall binding affinity. The robustness of this defect-insensitive adsorption mechanism is further confirmed by control simulations under physiologically relevant ionic strength (0.15-M NaCl) and with hydrogenated outer sheet edges, both of which yield virtually identical binding thermodynamics (see supporting information). In summary, our work elucidates an adsorption mechanism on graphene that is intrinsically robust to common nanoscale imperfections. The binding of small hydrophobic molecules like LCA is dominated by the continuous hydrophobic surface, with defect perturbations being too localized to alter the global interfacial water structure and its associated thermodynamics. This insight provides a crucial guideline for designing graphene-based biomedical interfaces: predictable adsorption performance can be expected even for materials with inherent nanoscale defects, significantly simplifying their practical application.

Acknowledgement

Project supported by the National Natural Science Foundation of China (Grant No. 52072132).

References

[1] Li T, Ding N, Guo H Q, Hua R, Lin Z H, Tian H H, Yu Y, Fan D M, Yuan Z Y, Gonzalez F J and Wu Y 2024 *Cell Host Microbe* **32** 191
[2] Sato Y, Atarashi K, Plichta D R, *et al.* 2021 *Nature* **599** 458
[3] Li Y W, Gu F, Gu H T, Hu P, Liu H X and Cai D M 2022 *Metabolites* **12** 659
[4] Chen S, Hu Z R, Tang J B, Zhu H P, Zheng Y H, Xiao J D, Xu Y H, Wang Y, Luo Y, Mo X Y, Wu Y L, Guo J W, Zhang Y L and Luo H H 2024 *Commun. Biol.* **7** 465
[5] Su X M, Gao Y H and Yang R C 2023 *Front. Immunol.* **14** 1127743
[6] Xu W, Kong Y Y, Zhang T, Gong Z H and Xiao W J 2023 *J. Sci. Food Agric.* **103** 1283
[7] Qu Q, Chen Y, Wang Y, *et al.* 2025 *Nature* **643** 201
[8] Qu Q, Chen Y, Wang Y, *et al.* 2025 *Nature* **643** 192
[9] You R, Liu Y Q, Hao Y L, Han D D, Zhang Y L and You Z 2020 *Adv. Mater.* **32** 1901981
[10] Olabi A G, Abdelkareem M A, Wilberforce T and Sayed E T 2021 *Renewable Sustainable Energy Rev.* **135** 110026
[11] Sang M, Shin J, Kim K, Li B and Yu K J 2019 *Nanomaterials* **9** 374
[12] Chen X K and Chen K Q 2020 *J. Phys.: Condens. Matter* **32** 153002
[13] Korkmaz S and Kariper I A 2020 *J. Energy Storage* **27** 101038
[14] Zhao H, Ding R H, Zhao X, Li Y W, Qu L L, Pei H, Yildirimer L, Wu Z W and Zhang W X 2017 *Drug Discovery Today* **22** 1302
[15] Song S J, Shen H, Wang Y L, Chu X H, Xie J, Zhou N L and Shen J 2020 *Colloids Surf. B* **185** 110596
[16] Luo S Y, Chen X, He Y H, Gu Y Q, Zhu C Z, Yang G H and Qu L L 2021 *J. Mater. Chem. B* **9** 6129
[17] Yang K, Feng L Z and Liu Z 2016 *Adv. Drug Delivery Rev.* **105** 228
[18] Song Y, Luo Y N, Zhu C Z, Li H, Du D and Lin Y H 2016 *Biosens. Bioelectron.* **76** 195
[19] Wang S and Luo X 2025 *ACS Omega* **10** 5593
[20] Maity T, Kumar Y, Deb A K S, Sheikh M A and Maiti P K 2025 *Langmuir* **41** 13811
[21] Ma H S, Chen J G, Fang H P and Lei X L 2021 *Chin. Phys. B* **30** 106806
[22] Bhatt M D, Kim H and Kim G 2022 *RSC Adv.* **12** 21520
[23] Gao D, Li B Y, Yang Y M, Qu Y Y, Li Y Q, Zhao M W, Liu Y, Liu X D and Li W F 2021 *J. Phys. Chem. B* **125** 2833
[24] López-Polin G, Gómez-Navarro C, Parente V, Guinea F, Katsnelson M I, Pérez-Murano F and Gómez-Herrero J 2015 *Nat. Phys.* **11** 26
[25] Dong Y, Zhang S, Du X, Hong S, Zhao S N, Chen Y X, Chen X H and Song H H 2019 *Adv. Funct. Mater.* **29** 1901127
[26] Liu L L, Qing M Q, Wang Y B and Chen S M 2015 *J. Mater. Sci. Technol.* **31** 599
[27] Zhang Y, Jia L G, Chen Y Y and Wang Y L 2022 *Chin. Phys. B* **31** 087301

[28] Wei S, Zou X Q, Tian J Y, Huang H, Guo W and Chen Z 2019 *J. Am. Chem. Soc.* **141** 20335
[29] Panczyk T, Nieszporek J and Nieszporek K 2022 *J. Phys. Chem. B* **126** 6671
[30] Mohammadi M M, Bavi O and Jamali Y 2023 *J. Mol. Graphics Modell.* **122** 108467
[31] Wang M H, Wang Q, Lu X, Wang K F, Fang L M, Ren F Z, Lu G M and Zhang H P 2017 *J. Phys. Chem. B* **121** 7907
[32] Zhang B Q and Shao Z G 2023 *Physica E* **146** 115547
[33] Zhang B W, Zhang B Q, Shao Z G and Wu X Q 2024 *Chin. Phys. B* **33** 118102
[34] Zhang B W, Zhang B Q and Shao Z G 2024 *Langmuir* **40** 22540
[35] Chen J, Xu E Z, Wei Y, Chen M H, Wei T and Zheng S Z 2022 *Langmuir* **38** 10817
[36] Li B Y, Bell D R, Gu Z L, Li W F and Zhou R H 2019 *Carbon* **146** 257
[37] Zuo G, Zhou X, Huang Q, Fang H P and Zhou R H 2011 *J. Phys. Chem. C* **115** 23323
[38] Lu T and Chen F W 2012 *J. Comput. Chem.* **33** 580
[39] Lu T 2024 *J. Chem. Phys.* **161** 082503
[40] Liu Z Y, Lu T and Chen Q X 2020 *Carbon* **165** 461
[41] Van der Spoel D, Lindahl E, Hess B, Groenhof G, Mark A E and Berendsen H J C 2005 *J. Comput. Chem.* **26** 1701
[42] Lindorff-Larsen K, Piana S, Palmo K, Maragakis P, Klepeis J L, Dror R O and Shaw D E 2010 *Proteins Struct. Funct. Bioinf.* **78** 1950
[43] Humphrey W, Dalke A and Schulten K 1996 *J. Mol. Graphics* **14** 33
[44] Jorgensen W L, Chandrasekhar J, Madura J D, Impey R W and Klein M L 1983 *J. Chem. Phys.* **79** 926
[45] Hess B, Bekker H, Berendsen H J and Fraaije J G 1997 *J. Comput. Chem.* **18** 1463
[46] Essmann U, Perera L, Berkowitz M L, Darden T, Lee H and Pedersen L G 1995 *J. Chem. Phys.* **103** 8577
[47] Darden T, York D and Pedersen L 1993 *J. Chem. Phys.* **98** 10089
[48] Bussi G, Donadio D and Parrinello M 2007 *J. Chem. Phys.* **126** 014101
[49] Berendsen H J C, Postma J P M, van Gunsteren W F, DiNola A and Haak J R 1984 *J. Chem. Phys.* **81** 3684
[50] Valdés-Tresanco M S, Valdés-Tresanco M E, Valiente P A and Moreno E 2021 *J. Chem. Theory Comput.* **17** 6281